Continuous rainfall simulation: 1. A regionalized subdaily disaggregation approach

Seth Westra,[1] Rajeshwar Mehrotra,[2] Ashish Sharma,[2] and Ratnasingham Srikanthan[3]

Received 28 January 2011; revised 5 December 2011; accepted 13 December 2011; published 25 January 2012.

[1] This paper is the first of two in the current issue that presents a framework for generating continuous (uninterrupted) rainfall sequences at both gaged and ungaged point locations. The ultimate objective is to present a methodology for stochastically generating continuous subdaily rainfall sequences at any location such that the statistics at a range of aggregation scales are preserved. This first paper presents a regionalized nonparametric daily disaggregation model in which, conditional on a daily rainfall amount and previous- and next-day wetness states at the location of interest, subdaily fragments are resampled using continuous records at nearby locations. The second paper then focuses on a regionalized daily rainfall generation model.To enable the substitution of subdaily rainfall at nearby locations for subdaily rainfall at the location of interest, it is necessary to identify locations with "similar" daily to subdaily scaling characteristics. We use a two-sample, two-dimensional Kolmogorov-Smirnov (K-S) test to identify whether the daily to subdaily scaling relationships are statistically similar between all possible station pairs sampled from 232 gages located throughout Australia. This step is followed by a logistic regression to determine the influence of the covariates of latitude, longitude, elevation, and distance to the coast on the probability that the scaling at any two locations will be similar. The model is tested at five locations, where recorded subdaily data was available for comparison, and results indicate good model performance, particularly in preserving the probability distribution of extremes and the antecedent rainfall prior to the storm event.

Citation: Westra, S., R. Mehrotra, A. Sharma, and R. Srikanthan (2012), Continuous rainfall simulation: 1. A regionalized subdaily disaggregation approach, *Water Resour. Res.*, *48*, W01535, doi:10.1029/2011WR010489.

1. Introduction

[2] Continuous (uninterrupted) sequences of subdaily rainfall is an important source of information for many hydrological applications, with fine-timescale rainfall often used as an input in the design of urban storm water systems, the simulation of environmental flows in small catchments, and the modeling of short-duration floods. In particular, the use of continuous sequences for this latter application has been the subject of much research [*Blazkova and Beven*, 2002; *Boughton and Droop*, 2003; *Cameron et al.*, 2000; *Lamb and Kay*, 2004], as it provides a viable means of accounting both for the "flood-producing" rainfall event itself as well as the antecedent rainfall in the hours, days, weeks, and months prior to the event, with both factors potentially having a significant bearing on the resulting flood estimates [*Kuczera et al.*, 2006; *Pui et al.*, 2011a].

[3] Compared to daily rainfall records, however, historical records of subdaily rainfall are usually more sparsely sampled in space, of shorter duration, and also often contain a greater percentage of missing data. To address the paucity of recorded subdaily records, a range of approaches has been developed for synthetically generating continuous subdaily rainfall sequences. These include multiscaling models, such the canonical and microcanonical cascades family of models, which are based on the observation that rainfall patterns exhibit "self-similarity" at a range of timescales, enabling information on coarse-scale rainfall to be used to describe behavior at finer timescales [*Gupta and Waymire*, 1993; *Lovejoy and Schertzer*, 1990; *Marshak et al.*, 1994; *Menabde et al.*, 1997; *Schertzer and Lovejoy*, 1987]. An alternative is the Poisson cluster suite of models, which simulate rainfall using a storm Poisson arrivals process [*Cowpertwait et al.*, 2007, 1996; *Koutsoyiannis and Onof*, 2001; *Rodriguez-Iturbe et al.*, 1987, 1988; *Verhoest et al.*, 1997]. Two popular implementations of this class of model are the Bartlett-Lewis and Neyman-Scott rectangular pulse models, with both having been used widely in research and engineering practice [e.g., *Frost et al.*, 2004]. Finally, nonparametric resampling models have been developed which avoid making strong assumptions as to the underlying distribution of the rainfall [e.g., *Lall and Sharma*, 1996; *Nowak et al.*, 2010; *Sharma et al.*, 1997; *Snavidze*, 1977; *Tarboton et al.*, 1998], by drawing "fragments"

[1]School of Civil, Environmental, and Mining Engineering, University of Adelaide, South Australia, Australia.
[2]School of Civil and Environmental Engineering, University of New South Wales, Sydney, New South Wales, Australia.
[3]Water Division, Australian Bureau of Meteorology, Melbourne, Victoria, Australia.

0043-1397/12/2011WR010489

from instrumental data to form new stochastic rainfall sequences.

[4] A limitation of many of these approaches is the need for long, high-quality subdaily rainfall records as the basis for parameter estimation in the case of the multifractal and Poisson class of models, or for drawing the subdaily "fragments" in the case of the nonparametric algorithms described above. This is particularly unfortunate given that the absence of long continuous rainfall records provides one of the principal justifications for continuous simulation, with the solution to this problem usually involving the development of "regionalized" approaches that make use of subdaily data within a broader spatial domain in the vicinity of the location of interest.

[5] The majority of work on such regionalized approaches has focused on the Poisson cluster family of models. For example, *Cowpertwait et al.* [1996] and *Cowpertwait and O'Connell* [1997] developed a regionalized Neyman-Scott Rectangular Pulse (NSRP) model for generating sequences of hourly rainfall data across the UK, by regressing the NSRP parameters on site variables obtained from a relief map of the UK (including: elevation, north-south distance, east-west effect, and distance to coast). *Cowpertwait et al.* [1996] also developed a disaggregation model that allows historical or generated hourly data to be disaggregated into totals for shorter time intervals. An alternative approach was proposed by *Gyasi-Agyei* [1999], who developed a regionalized version of the Gyasi-Agyei and Willgoose hybrid model based on the nonrandomized Bertlett-Lewis rectangular pulse and an autoregressive jitter [*Gyasi-Agyei and Willgoose*, 1997, 1999]. This approach uses observed daily statistics (namely dry probability, mean, and variance) and two regionalized subdaily parameter estimates, with promising results found in simulating subdaily rainfall in central Queensland, Australia. This model was extended to Australia-wide data by *Gyasi-Agyei* and *Parvez Bin Hahbub* [2007], and was found to be successful in simulating a range of statistics including extreme rainfall.

[6] In our two articles, we present an alternative regionalized framework for generating continuous subdaily rainfall sequences, drawing on the nonparametric resampling approaches developed by *Lall and Sharma* [1996] and a novel approach at defining regional similarity. Specifically, in this paper a nonparametric disaggregation approach will be described, in which subdaily rainfall "fragments" are randomly sampled from nearby pluviograph stations conditional on daily rainfall amounts at the location of interest. This is one of the first regionalized extensions to the method of fragments logic, and substantially expands the applicability of the method of fragments due to the relative abundance of high-quality daily rainfall data compared to subdaily rainfall records. We also modified the method of fragments logic to also consider previous- and next-day wetness stages, with this modification improving the continuity of the resampled-subdaily fragments, and it is made possible because of the greater sample size brought about by using multiple nearby records.

[7] In the second paper, an algorithm is developed for generating daily rainfall sequences at ungaged locations, once again being informed by data from nearby gaged locations. The combination of these two algorithms allows for a complete regionalized framework for generating point-based continuous rainfall sequences at any desired location. Detailed testing of these algorithms is conducted with an emphasis on evaluating the extent to which the methods capture both the distribution of extreme rainfall and the antecedent rainfall leading up to the extreme event, reflecting the likely applicability of these techniques for flood estimation practice.

[8] The remainder of this paper is structured as follows. In section 2 we provide an overview of Australia's continuous rainfall record. This is followed in section 3 by a description of the proposed methodology, including the statistics used to determine the similarity between daily/subdaily rainfall relationships at any two locations. Results are presented in section 4, including a preliminary analysis of the viability of the method at Sydney Airport, Australia, as well as more detailed results for five case study locations distributed throughout Australia. Finally, a discussion and conclusions are provided in section 5.

2. Data

[9] Continuous subdaily rainfall data were obtained from the Australian Bureau of Meteorology (www.bom.gov.au) at 1397 stations, in increments of 6 minutes. The location of each gaging station is shown in Figure 1, together with an indication of the length of record. The median record length of all stations was 9 yr, with only 101 stations having records longer than 40 yr, and an additional 331 stations have records of between 20 and 40 yr. Furthermore, the spatial distribution of the gaging stations is not homogeneous, with a high density of gages in the populated regions particularly along the eastern coastal fringe of Australia, and lower density elsewhere. In contrast, there are 17,451 daily-read gaging stations in Australia, of which 2708 locations stations have records longer than 20 yr, and 1768 stations which have more than 40 yr of record. This asymmetry in data availability between daily and subdaily records highlights the potential benefits of developing a regionalized disaggregation approach using the conditional relationship between daily and subdaily rainfall.

[10] The number of gaging stations with continuous rainfall records are plotted against the year of record in Figure 2. As can be seen, only a small number of gaging stations were available in the early twentieth century (the longest available record in Australia being from Melbourne Regional Office, gage number 086071, with data from 1873), with significant increases in recording density apparent in the 1960s. To limit the effects of possible temporal variability in the daily/subdaily characteristics, the remainder of the paper only considers records between 1970 and 2005 with less than 20% of the record classified as "missing," with a total of 232 stations meeting this criterion. "Missing" data was defined as data which was flagged as either missing or presented as an accumulation over previous time steps, and in these cases the full day of record was removed from the analysis. As will be discussed further below, the proposed method is relatively insensitive to missing data.

3. Methodology

3.1. Regionalized Method of Fragments Algorithm

[11] The method of fragments is a well-known resampling algorithm for generating continuous rainfall sequences

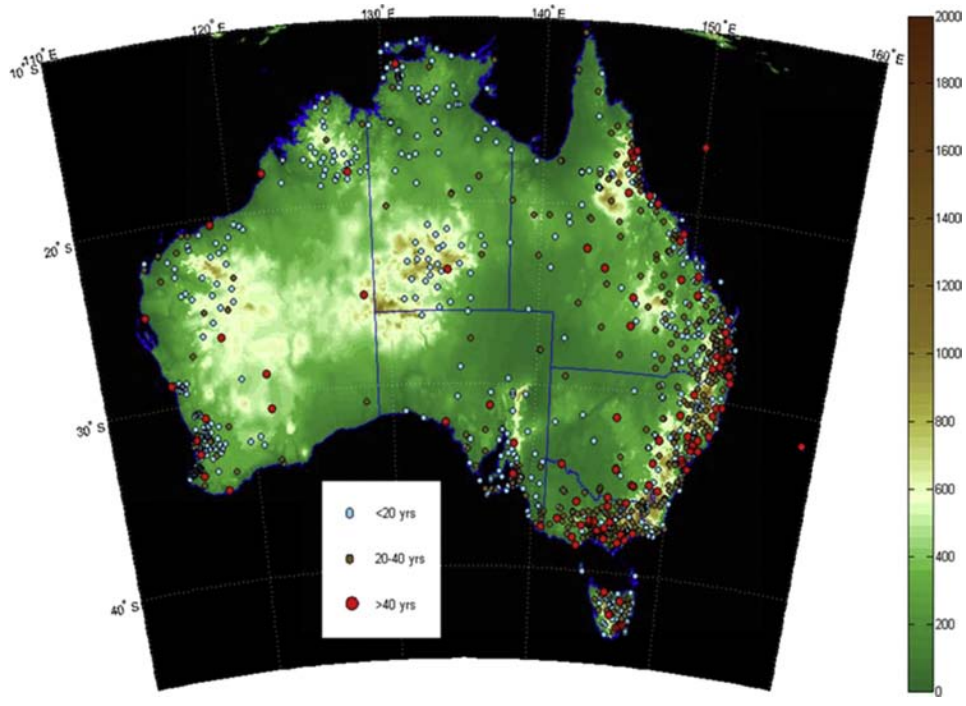

Figure 1. Spatial coverage and record length of the Australian subdaily pluviograph record.

[*Lall and Sharma*, 1996; *Nowak et al.*, 2010; *Sharma and Srikanthan*, 2006; *Sharma et al.*, 1997; *Snavidze*, 1977; *Tarboton et al.*, 1998]. In this paper, we make two modifications to enable the method to be applied in a regionalized setting. The first and most important modification involves the development of a regionalized version in which, conditional on daily rainfall at the location of interest, fragments are sampled from a range of "nearby" locations. The second modification involves including a "state-based" logic in which fragments are drawn not only conditional on daily rainfall amounts, but also on whether the previous and next day are wet or dry. As will be discussed later, this second modification partially overcomes an issue with the conventional method of fragments related to continuity of the resampled-subdaily rainfall fragments when there are successive wet days, and is made possible here because of the greater sample size due to use of a larger number of nearby stations.

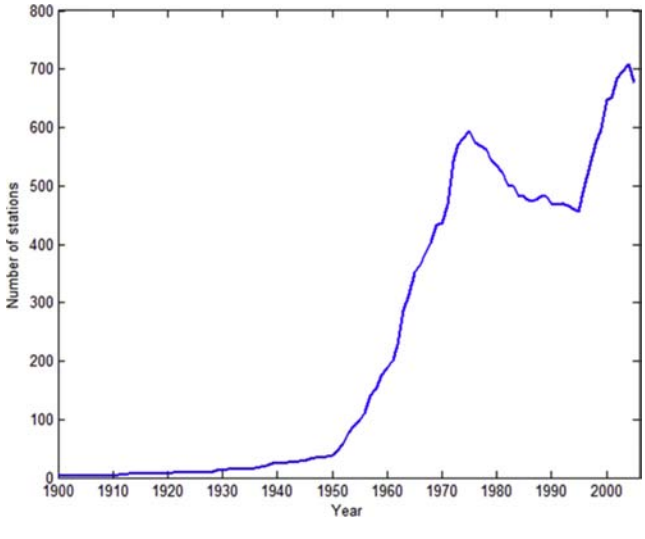

Figure 2. Number of Australia-wide pluviograph records against year of record, plotted from 1900.

[12] The algorithm for the adjusted method of fragments is presented here. The approach is also illustrated in Figure 3, with the steps in the algorithm matching the steps highlighted in the figure. The algorithm:

Step 1: Obtain a sequence of daily rainfall R_i^o at the location of interest, where subscript i indexes time and the superscript "o" refers to the target location (the location at which the continuous rainfall sequences are sought). The daily rainfall sequence can be obtained either from a historical record of daily rainfall at the target location, or alternatively from a daily stochastic generation algorithm such as the one described in our second paper.

Step 2: Obtain daily rainfall sequences at a range of "nearby" subdaily rainfall gages, via:

$$R_i^s = \sum_m X_{i,m}^s, \tag{1}$$

where $X_{i,m}^s$ represents the rainfall depth on day i and at subdaily time step m, at nearby station s. For the present study we have subdaily rainfall available in increments of 6 min, such that $m \in \{1, \ldots, 240\}$. We also obtain the subdaily fragments given by $fr_{i,m}^s = X_{i,m}^s / R_i^s$, which is a dimensionless version of the subdaily rainfall record.

Step 3: For each wet day $R_t^o > 0$, search for days with similar daily rainfall depth across all nearby stations $s = 1, \ldots, S$, where S represents the total number of nearby stations, across every year for which subdaily data is

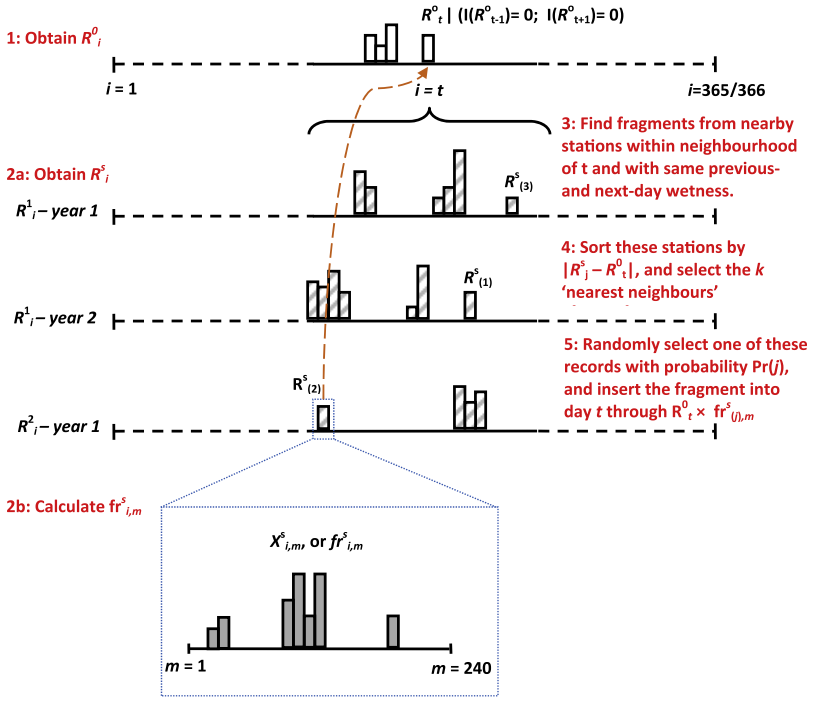

Figure 3. Illustration of the state-based method of fragments algorithm. The indicated steps correspond to the steps of the algorithm in section 3.1.

available. For example, if we consider 20 nearby stations which each have an average length of record of 9 yr, this would amount to a total of 180 yr of record. To preserve seasonality, we only look within a moving window of ±15 days centered on day t. In other words, if $t = 45$ (14 February), we search for days from $t = 30$ to $t = 60$. Furthermore, to account for continuity across the boundaries we only look at wet days with the same previous- and next-day wetness state (i.e., $\mathrm{I}[R^s_{i-1}] = \mathrm{I}[R^o_{t-1}]$ and $\mathrm{I}[R^s_{i+1}] = \mathrm{I}[R^o_{t+1}]$), where I( ) represents a binary indicator function defined as $\mathrm{I}(R) = 1$ for a wet day and $\mathrm{I}(R) = 0$ for a dry day.

Step 4: We use an index $j = 1, \ldots, n$ to refer to days which are within the moving window and have the same previous- and next-day wetness state, with the total number of days n being calculated across all the nearby stations S and across all years of record at each station. These days are ranked by absolute deviation in rainfall depth $|R^s_j - R^o_t|$, to construct a sorted series $R^s_{(j)}$ from the smallest absolute deviation to the largest, where the use of parentheses indicates that the data has been sorted. We find the k nearest neighbors $(j) = 1, \ldots, (k)$, with the value of k selected to ensure all the neighbors have an absolute deviation in rainfall depth of less than 10% of the at-site rainfall, up to a maximum of 10 nearest neighbors.

Step 5: Randomly draw from $R^s_{(j)}$ with probability:

$$P(j) = \frac{1/(j)}{\sum_{i=1}^{k} 1/i}, \tag{2}$$

where $P(j)$ represents the probability of selecting neighbor (j) [*Lall and Sharma*, 1996; *Mehrotra and Sharma*, 2006]. The selected fragment is then inserted into day R^o_t via $fr^s_{i,m} = X_{(j),m} \times R^o_t$.

[13] This completes the algorithm for the regionalized method of fragments. In total, there are three "tuning" parameters: the number of nearby stations S to include in the model, the number of nearest neighbors k, and the width of the moving window. Given the large amount of variability in record length from one subdaily rainfall station to the next, we let S vary such that sufficient stations were selected to have at least 250 yr of record from which to sample. The value of $k = 10$ was chosen as this ensured the daily total rainfall for each fragment was within a relatively small tolerance of R^o_t, while still ensuring a significant amount of induced sampling variability. Sensitivity to each of these turning parameters was evaluated and found to be fairly limited. Finally, the width of the moving window was selected so as to ensure that samples were all drawn from the same time of year.

[14] Although the overall approach is conceptually simple, the challenge is to define the neighborhood from which to sample the S pluviograph records. The basis for identifying whether the daily-to-subdaily scaling at two locations is similar and thus substitutable is described below.

3.2. Daily-to-Subdaily Scaling

[15] To enable substitution of subdaily fragments from one station to another, one needs to ensure that for any day t, the conditional relationship between the daily rainfall amount R_t and the full sequence of subdaily rainfall $X_{i,m}$ are statistically similar at both the target station and the nearby stations. This can be expressed as,

$$f(X^s_{i,m}|R^s_t) = f(X^o_{i,m}|R^o_t) \tag{3}$$

for all m and t, where $f(.|.)$ is used to express a conditional probability density function. Given the difficulty of constructing

separate conditional density functions for 240 separate increments of subdaily rainfall, as well as the fact that for any wet day R_t there is a high probability that any subdaily rainfall increment $X_{t,m}$ has no rainfall, we modify equation (3) as follows:

$$f(Y_t^s|R_t^s) = f(Y_t^o|R_t^o), \tag{4}$$

where Y_t^s and Y_t^o represent scalar attributes of $X_{t,m}^s$ and $X_{t,m}^o$ for each day of record, respectively. The attributes to be considered include:

[16] Maximum intensity: for each wet day, what is the maximum 6-, 12-, 30-, 60-, 120-, 180-, and 360-min duration storm burst expressed as a fraction of the total rainfall amount for that day?

[17] Fraction of zeros: for each day, what is the fraction of 6-min time steps with no rainfall?

[18] Maximum intensity timing: for each wet day, what is the time of day when the maximum 6-, 12-, 30-, 60-, 120-, 180-, and 360-min duration storm burst occurs?

[19] In combination, these scalar attributes are expected to cover most of the information on the scaling and timing behavior between daily rainfall and the fragments.

[20] To illustrate these concepts, we present in Figure 4 the joint probability plot of daily rainfall and the maximum 12-min storm burst at three locations in Australia: Hobart, Sydney, and Darwin. These locations were selected as they have distinctly different climatology, with Hobart located in the south of Tasmania being one of the most southerly pluviograph records, Darwin in the Northern Territory being one of the most northerly pluviograph records, and Sydney being situated along the Australian east coast.

[21] As can be seen in the daily rainfall histogram (Figure 4, lower panel), the marginal probabilities of daily rainfall at each station are distinctly different. For example, Darwin has a high probability of high daily rainfall amounts (the majority of rain days having >10 mm rainfall), whereas Hobart has a large number of rain days with relatively little rainfall, with most days having significantly less than 10 mm over the entire day. It should be emphasized, however, that our interest here is not on this marginal

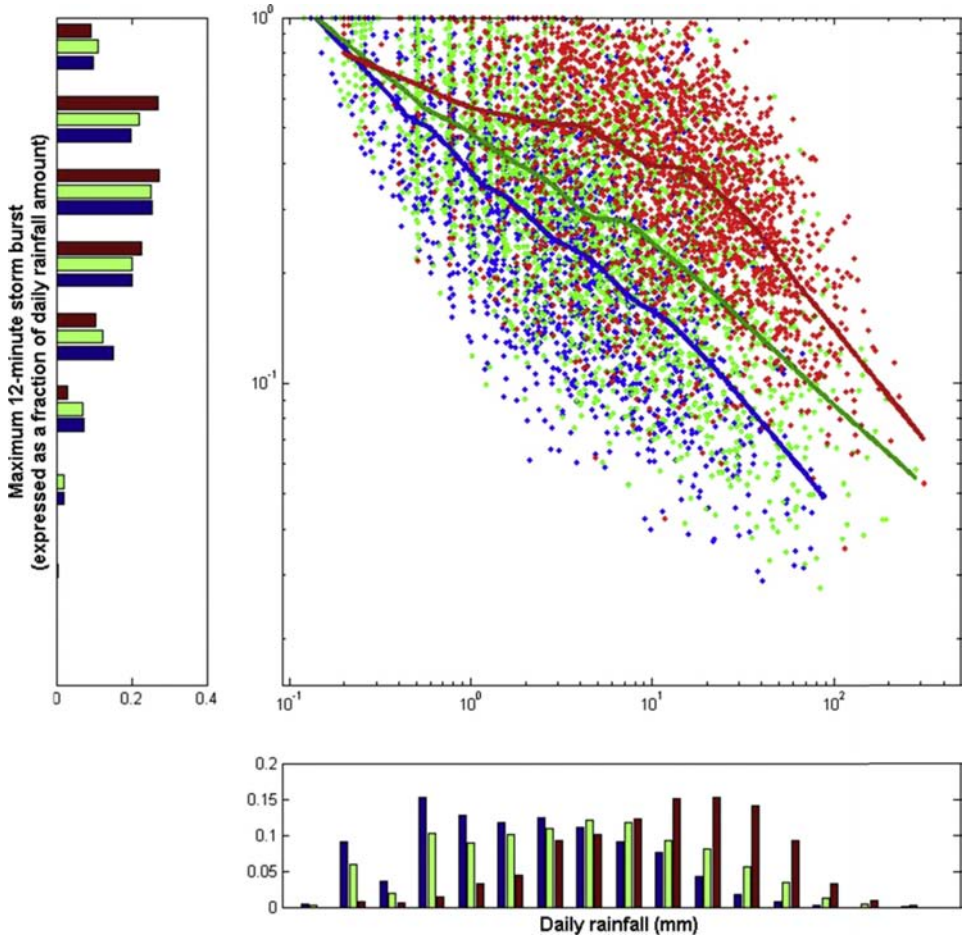

Figure 4. Scatterplot with daily rainfall and an attribute of subdaily rainfall (the maximum 12-min storm burst expressed as a fraction of the total daily rainfall) at three locations in Australia: Hobart (blue), Sydney (green), and Darwin (red). Histograms of daily rainfall and the maximum 12-min storm burst are provided in the bottom and left figure panels, respectively, for each of the three locations. The solid lines are loess smoothers of the observations, and are provided for visualization purposes only.

distribution; rather, we wish to know, conditional on some daily rainfall amount, whether the subdaily rainfall properties are the same at any two locations. To determine whether this is the case, we started by plotting a loess smoother [*Hastie et al.*, 2009] with support of 25% of the sample to represent the conditional expected value of the maximum 12-min storm burst as a function of daily rainfall.

[22] It is evident that the fraction of daily rainfall contained in the maximum 12-min storm burst varies as a function of the daily rainfall amount. This is unsurprising, as intuitively one would expect that for small daily rainfall amounts, a smaller percentage of the day would be wet, and therefore there is a greater chance that the maximum 12-min storm burst contains a large portion of the daily rainfall. Interestingly, however, the loess smoother highlights that the relationship between daily rainfall and subdaily rainfall is on average very different at the three locations, with Darwin typically having a greater fraction of the daily rainfall contained within the maximum 12-min storm burst than Hobart. This suggests that even if both stations have the same daily total rainfall amount, Darwin is more likely to have that rainfall distributed over a number of short-duration, high-intensity rainfall events compared with Hobart whose rainfall is more likely to be spread evenly over the day, with these results appearing sensible given the tropical nature of Darwin climate. Although figures are not provided here, consistent conclusions can be drawn from considering other durations, as well as the fraction of each wet day that does not experience rainfall.

3.3. Defining Similarity

[23] We now wish to devise a metric to determine whether the conditional distributions in equation (4) and illustrated in Figure 4 are, in fact, statistically equivalent. To simplify the analysis, rather than focus on the conditional distribution we consider whether the joint distribution of Y and R at any two stations is equivalent, given by

$$f(Y^s, R^s) = f(Y^o, R^o). \tag{5}$$

[24] This is a stricter criterion compared to the conditional distribution in equation (4), because two locations having equivalent joint distributions imply that the conditional distribution must also be equivalent, although the opposite is not necessarily true. (One can easily imagine two samples having an equivalent distribution of subdaily rainfall conditional on daily rainfall amount, but different marginal distribution for the daily rainfall amount, and therefore different joint distributions.)

[25] To test the hypothesis that the joint distribution between daily rainfall and some attribute of subdaily rainfall at any two locations are statistically similar, we use a two-dimensional, two-sample Kolmogorov-Smirnov (K-S) test. This represents a generalization of the better known one-dimensional K-S test [*Press et al.*, 1992], and was developed by *Fasano and Franceschini* [1987]. The basis of the two-dimensional generalization is that although a cumulative distribution function is not well defined over more than one dimension, the integrated probability in each of four quadrants around some point (x_i, y_i) in some arbitrary x- and y-dimensions provides a reasonable approximation. The two-dimensional K-S statistic D is the maximum difference (ranging over both data points and quadrants) of the integrated probabilities, and is given by [*Press et al.*, 1992]:

$$\Pr(D > \text{observed}) = Q_{KS}\left(\frac{\sqrt{N}D}{1+\sqrt{1-r^2\left[0.25-\frac{0.75}{\sqrt{N}}\right]}}\right), \tag{6}$$

where

$$N = \frac{N_1 N_2}{N_1 + N_2}, \tag{7}$$

with N_1 and N_2 representing the size of samples 1 and 2, respectively. In calculating the probability that the K-S statistic, as described in equation (6), is above some defined level under the null hypothesis that the two samples are from the same population, it is necessary to evaluate the function:

$$Q_{KS}(\lambda) = 2\sum_{j=1}^{\infty}(-)^{j-1}e^{-2j^2\lambda^2}. \tag{8}$$

[26] This allows for the estimation of the probability that the joint distribution of two different data sets are statistically similar, with further details on this statistic provided by *Press et al.* [1992].

3.4. Predictive Model for Statistical Similarity

[27] In section 3.3 we described a metric for determining whether the joint distribution between daily rainfall amounts and attributes of subdaily rainfall, as illustrated in Figure 4, is statistically similar. As discussed earlier, to use this information to extend the continuous simulation approach to locations where pluviograph data is unavailable, it is necessary to draw subdaily fragments from nearby stations conditional on daily rainfall at the target location. As such, we now wish to determine: What are the factors that will influence whether the daily-to-subdaily scaling at two stations will be similar?

[28] To answer this question, we consider each possible pairing of the 232 pluviograph stations with at least 30 years of data, totaling 26,796 station pairs, and calculate the two-sample, two-dimensional K-S statistic for each pair of stations and subdaily rainfall attributes. We use a 5% significance level to evaluate whether two stations are similar, and then consider how the probability that any two stations are similar varies as a function of a range of possible covariates, including difference in latitude, longitude, distance to coast, and elevation between each station pair. These predictors, summarized in Table 1, comprise a range of easily measurable physiographic characteristics, which might be expected to influence the similarity between two stations. Seasonal variations in the daily-to-subdaily rainfall relationship are accommodated by formulating a separate model for each season of the year.

[29] Thus, we have a set of continuous predictors represented by $\mathbf{V}$ (dimension 26,796 $\times$ 5) which we wish to model against a binomial response represented by $\mathbf{u}$ of

Table 1. Predictors Used for the Logistic Regression Model Described in Equations (9) and (10)[a]

Predictor	Units	Description/Comments
Diff_lat	Degrees (expressed as a decimal)	Difference in latitude between each station pair, calculated as abs(Lat_1–Lat_2)
Diff_lon	Degrees (expressed as a decimal)	Difference in longitude between each station pair, calculated as abs(Lon_1–Lon_2)
Diff_lat × Diff_lon	Degrees (expressed as a decimal)	Interaction term, which would be greater than zero if it is the distance between stations, rather than the sum of the latitude and longitude, which is the dominant predictor.
Diff_dist_coast (normalized)	Dimensionless	Difference in distance to coast between each station pair, normalized by the average distance to coast for the station pair, calculated as abs($dist_1$–$dist_2$)/ mean($dist_1$, $dist_2$).
Diff_elev	Meters	Difference in elevation between each station pair, calculated as abs($Elev_1$–$Elev_2$)

[a]The prefix "Diff_" emphasizes that it is the difference in each of the predictors between stations that is considered, rather than the absolute value.

length 26,796 (where $\mathbf{u} \in \{0, 1\}$ represents the cases where the scaling between daily and subdaily rainfall at two stations are statistically different and similar, respectively, as calculated by the Kolmogorov-Smirnov test described in section 3.2). This relationship can be modeled using a logistic regression, in which

$$\Pr(u = 1) = \text{logit}(z) = \frac{e^z}{e^z + 1} \tag{9}$$

transforms the continuous predictor variables to the range [0,1] as required when modeling a binomial response. In this equation, z is defined as

$$z = \beta_0 + \beta_1 \mathbf{v}_1 + \ldots + \beta_5 \mathbf{v}_5, \tag{10}$$

with β representing the regression coefficients. The results of the logistic regression model are shown in Figure 5, plotted against the difference in latitude. The results are presented for four attributes of subdaily rainfall: 6 min maximum storm burst, 1 h maximum storm burst, fraction of day with no rainfall, and time of day with the maximum 6-min storm burst. Note that for the time attribute, we are only considering the marginal distribution of the time of day when the maximum 6-min storm burst occurs, rather than a joint density.

[30] As can be seen in Figure 5, with the exception of the fraction of zeros measured by the K-S statistic, there is a chance between 40% and 60% that the joint distribution of daily rainfall and each of the attributes are statistically similar provided that the difference in latitude is small, with the probability decreasing rapidly with increasing difference in latitude. This is interesting, as no account is made of any other physiographic information, so that stations may be located in opposite sides of the continent, or at very different elevations, and yet still have close to a 50% chance of having the same scaling between daily and subdaily rainfall, provided the latitude is the same. The joint distribution of daily rainfall and fraction of zeros has the lowest probability of being statistically similar between station pairs, with a chance of ~22% that two stations will have the same joint dependence, assuming they are at the same latitude.

[31] Consideration of just a single covariate – difference in latitude – as in latitude as the only factor influencing the similarity between stations ignores other physiographic information which may be important. As such, we extend this model to a multivariate logistic regression setting to consider the influence of each of the plausible predictors mentioned above. The conceptual basis for this approach is illustrated in Figure 6. Given a target location of interest, we wish to define a zone for which the probability that daily-to-subdaily scaling at two stations are statistically similar is greater than a predefined threshold. This zone is described by contours of equal probability, with the probability decreasing linearly (in the logistic transformed space) in each of the dimensions of the regression model. The shapes of the contours are defined by the logistic regression coefficients. In the idealized example in Figure 6, we represent the case where the probability of two stations being statistically similar decreases at a faster rate in the latitude dimension compared to the longitude dimension. Furthermore, the location of the target station is slightly offset from the center of the contours, this being governed by the influence of the relative difference in distance to the coast.

[32] The results of this multivariate regression are presented in Table 2, and once again plotted for the summer

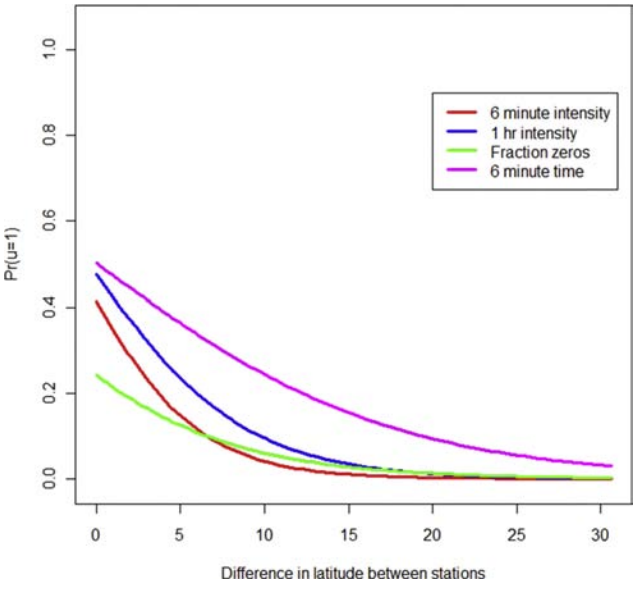

Figure 5. Logistic regression results against a single predictor (difference in latitude) and four responses representing different subdaily attributes. The responses have been calculated using the two-sample two-dimension Kolmogorov-Smirnov test statistic.

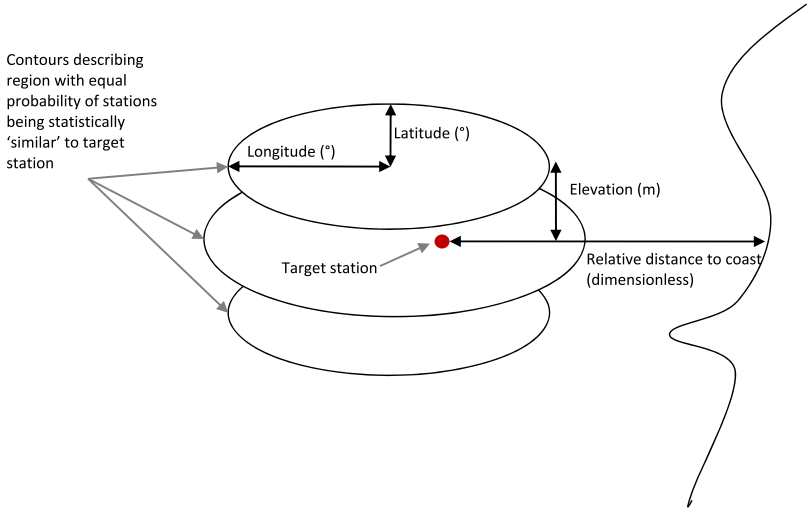

Figure 6. Diagrammatic representation of logistic regression results. The response is the probability that the joint distribution of daily rainfall amount and some attribute of subdaily rainfall at a "nearby" station is statistically similar to the target station. The predictors are the difference in latitude, longitude, latitude × longitude, elevation, and a normalized distance to coast, with the logistic regression coefficients determining the relative decrease in the probability that two stations are similar in each of these dimensions.

months against latitude in Figure 7, with the remaining predictors held at zero. As can be seen, the results in Figure 7 show notable improvements in the probability that two stations are equal compared to Figure 5, because we are now plotting the influence of latitude assuming that differences in longitude, elevation, and relative distance to coast are all zero. In fact, with the exception of the fraction of zeros, the results show that for small values of each of the predictors there is between a 60% and 70% probability that the daily-to-subdaily joint probability distributions are statistically similar. Once again, the fraction of zeros is the most challenging statistic in terms of maintaining similarity, with only a chance of 40% that two stations have the same scaling, assuming all the predictors are zero.

[33] It should be emphasized that this is in many ways a conservative estimate as we consider the subdaily attributes (e.g., fraction of zeros, 6-min rainfall intensity), which are the most challenging to capture from daily data alone. Even more importantly, as can be seen in the example of Figure 4, the number of samples in each bivariate distribution is large (30 years of data, 90 days per season, and ∼30% of days being wet days yields ∼800 wet days), such that the 95% confidence intervals are very narrow (as the width of the confidence intervals is governed by sample size).

Table 2. Logistic Regression Coefficients[a]

Season	Subdaily Rainfall Attribute	Logistic Regression Coefficients					
		Intercept	Latitude	Longitude	Latitude × Longitude	Distance Coast	Elevation
DJF	6 min intensity	0.426	−0.345	−0.0377	0.0064	−0.186	−0.00089
DJF	1 h intensity	0.823	−0.333	−0.0425	0.0093	−0.231	−0.00075
DJF	Fraction of zeros	−0.375	−0.253	−0.0318	0.0075	−0.242	−0.00065
DJF	6 min time	0.979	−0.137	−0.0099	0.0022	−0.453	−0.00141
MAM	6 min intensity	−0.067	−0.192	−0.0065	NS	−0.218	−0.00130
MAM	1 h intensity	0.308	−0.178	−0.0074	NS	−0.107	−0.00098
MAM	Fraction of zeros	−0.806	−0.157	−0.0105	0.0025	−0.165	−0.00060
MAM	6 min time	1.256	−0.140	−0.0226	−0.0034	−0.227	−0.00092
JJA	6 min intensity	−0.197	−0.097	−0.0110	0.0034	−0.096	−0.00198
JJA	1 h intensity	0.471	−0.102	−0.0204	0.0033	NS	−0.00335
JJA	Fraction of zeros	−0.365	−0.073	−0.0171	0.0031	−0.101	−0.00116
JJA	6 min time	2.078	−0.098	−0.0321	0.0037	−0.156	−0.00069
SON	6 min intensity	0.474	−0.387	−0.0722	0.0129	NS	−0.00146
SON	1 h intensity	0.824	−0.325	−0.0835	0.0135	NS	−0.00132
SON	Fraction of zeros	−0.382	−0.239	−0.0623	0.0104	−0.087	−0.00095
SON	6 min time	1.028	−0.162	−0.0287	0.0042	−0.317	NS

[a]All predictors were found to be statistically significant (usually with a p-value <0.001 level), with the exception of several predictors labeled as NS (not significant). Seasons include December-January-February (DJF), March-April-May (MAM), June-July-August (JJA) and September-October-November (SON).

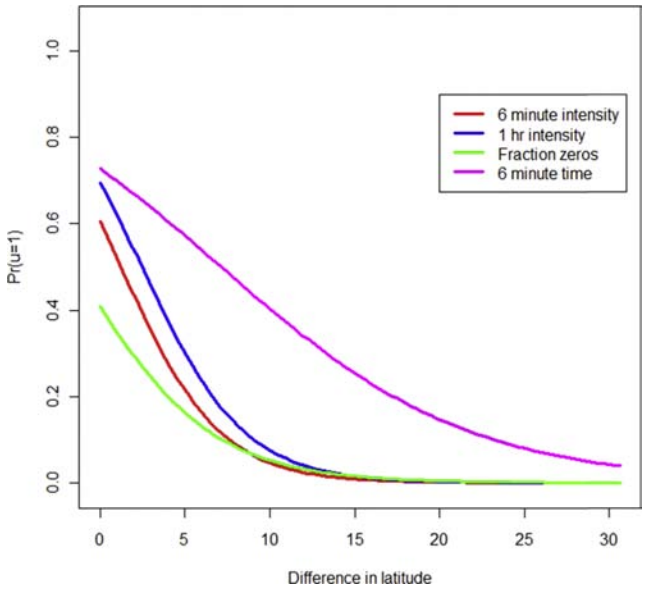

Figure 7. As per Figure 5, except the results represent the outcomes of the full multivariate regression. The probability that daily to subdaily scaling is statistically similar is once again plotted against difference in latitude, however, now all the remaining predictors are held at zero.

4. Results

4.1. Identifying "Nearby" Stations: Application to Sydney Airport

[34] We start by demonstrating a single application of the approach at one location: Sydney Airport (gage number 066037). This location represents a relatively long-record pluviograph station, and therefore provides a useful record for verification of the method.

[35] The approach to identifying "nearby" stations is as follows:

[36] (1) For all 1396 pluviograph stations in Australia (excluding the Sydney Airport gage), calculate each of the regression predictors identified in Table 1; namely, difference in latitude, longitude, latitude times longitude, elevation, and normalized distance to the coast, relative to the Sydney Airport station.

[37] (2) Having developed the 1396 $\times$ 5 predictor matrix, apply the regression model presented in equations (9) and (10) using the regression coefficients shown in Table 2 for each season and attribute to calculate the probability $\Pr(u = 1)$.

[38] (3) For each season and attribute, separately rank the probabilities from highest to lowest.

[39] (4) For each season calculate the average rank for each station across all attributes.

[40] (5) Select the S lowest-ranked stations for inclusion in the disaggregation model.

[41] This algorithm yields different choices of stations for each season, as physiographic influences may vary depending on the dominant synoptic systems occurring at different times of the year. It is noted that the selection of the size of S represents a somewhat subjective decision, as larger values of S increase the probability of selecting stations which are statistically different to the target station, whereas smaller values of S will result in small sample sizes. For this case, we selected $S = 13$, resulting in a total of 250 yr of data distributed over the 13 stations.

[42] The 13 lowest-ranked stations for the summer season are shown in Figure 8. As expected, the lowest-ranked stations (i.e., those with the greatest chance of being similar

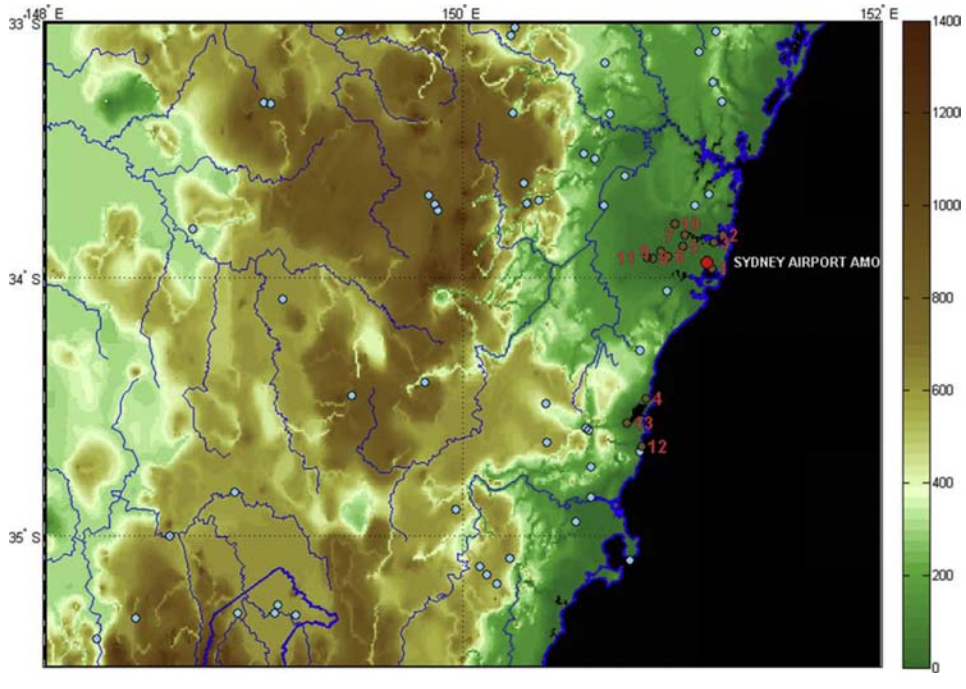

Figure 8. Sydney Airport (large red dot) and nearby pluviograph stations (blue and brown dots). The highest-ranked 13 pluviograph stations (totaling ~250 yr of pluviograph data) based the full logistic regression model are shown as brown dots, with the associated ranking.

to Sydney Airport) are those which are most proximate to this station, generally within a small distance to coast, and all are at low coastal elevations. In this case, therefore, the stations appear to be selected over a wide range of latitudes, which is probably due to the strong increases in elevation and relative distance to the coast with changing longitude.

4.2 Model Evaluation

[43] We now repeat the process of identifying nearby stations at five locations across Australia each having more than 50 yr of pluviograph data, representing a diversity of climate zones. These stations are shown in Table 3. Having identified the pool of nearby stations from which to draw the fragments, we apply the approach described in algorithm 1 to draw subdaily rainfall fragments from nearby stations conditional on at-site daily rainfall, and compare these sequences to the at-site pluviograph records. For comparison purposes, we also generated results using the algorithm but with at-site results only, and presented these alongside the regionalized results.

[44] It is emphasized that the use of a disaggregation model derived using observed daily rainfall sequences implies that the daily- and longer-timescale statistics will be identical to the observational data set. As such, the selection of evaluation statistics should focus on the capacity of the model to simulate rainfall at subdaily timescales. Reflecting the likely application of this model for flood estimation, the statistics considered here are based on: whether the model is capable of reproducing the extreme rainfall intensity; and whether the model captures the antecedent rainfall prior to the flood-producing rainfall event. In addition, several statistics have been calculated to determine the connectivity of rainfall events between successive wet days.

[45] Considering first the annual maxima statistics, we present in Figure 9 a plot of the annual maximum 6-min rainfall against the exceedance probability for both the observed data at the target location, as well as the results of 100 simulation runs with the same length of series as the original target pluviograph time series. The left column represents the results using at-site data as the basis for resampling, while the right column represents results using data from nearby records. The median and the 5th and 95th percentiles are calculated empirically from these 100 simulation runs, with the 5th and 95th percentile values measuring the degree of sampling variability induced by the stochastic generation algorithm.

[46] As can be seen, the observed data is generally within the sampling interval for most of the stations, with the exception of Alice Springs, for which the generated sequences tend to overestimate rainfall for all exceedance probabilities, and for Hobart in which the simulated sequences underestimate the low exceedance probability rainfall events. Interestingly, this is observed for both results using at-site data and nearby station data, highlighting that the issue is unlikely to be related to the regionalization procedure. In fact, a more thorough examination indicates that the annual maxima of the daily rainfall obtained using the daily rainfall record is on average slightly higher than the annual maxima of daily rainfall obtained from the subdaily rainfall record, due to the daily record being more complete (i.e., with less missing days) than the subdaily record. The issue is particularly notable for Alice Springs and Hobart, which both have a significant percentage of the pluviograph record classified as missing, such that resampling the subdaily fragments conditional to the daily rainfall record would be expected to yield simulated series which on average have higher annual maximum rainfall at both daily and subdaily durations.

[47] In addition to this issue, it was noted that the maximum largest 6-min value for the Hobart Airport record was well in excess of the simulated results, with this being noticeable for both the at-site and regionalized results. In particular, the maximum-recorded 6-min storm burst was 23.14 mm occurring on 24 April 1972, representing a very intense storm burst for such a high latitude. Aggregating the pluviograph record for that full day showed 192.2 mm falling, which contrasted with the daily station at the same location recording only 42.2 mm for that day. We also examined the nearest pluviograph and daily-read station pairing, namely gage number 94029 located 15.6 km from the Hobart Airport gage, and found the aggregated daily rainfall from the pluviograph to be 27.94 mm, compared with 27.9 mm from the daily rain gage at that same location. Furthermore, the maximum 6-min increment rainfall intensity was found to be 1.74 mm, substantially smaller than that recorded at Hobart Airport. This therefore indicates that a recording error probably occurred at the pluviograph gage at Hobart Airport.

[48] For both reasons, we suggest that the simulated results in this case may be more likely to reflect the precipitation patterns at each location compared with the observed subdaily record at those same locations, although this conclusion is unlikely to apply everywhere. Comparing the sampling intervals for the at-site and regionalized results, it can be seen that the regionalized intervals are generally smoother, and tend to widen for higher events. In contrast, the at-site results tend to have narrower sampling intervals for the events with the lowest exceedance probabilities, reflecting the small sample size from which to draw subdaily fragments for these large events. Therefore, rather

Table 3. Data Used to Test Continuous Simulation Model[a]

Station Airport	Gage Number	Start Year	Years of Observed Data	Latitude/Longitude	Köppen Climate Classification
Sydney	066037	1961	45	−33.9411/151.1725	Temperate (warm summer)
Perth	009021	1960	46	−31.9275/115.9764	Subtropical (dry summer)
Alice Springs	015590	1950	57	−23.7951/133.8890	Desert/grassland (hot, persistently dry)
Cairns	031011	1941	66	−16.8736/145.7458	Tropical (monsoonal)
Hobart	094008	1959	47	−42.8339/147.5033	Temperate (mild summer)

[a]All stations continue until 2009.

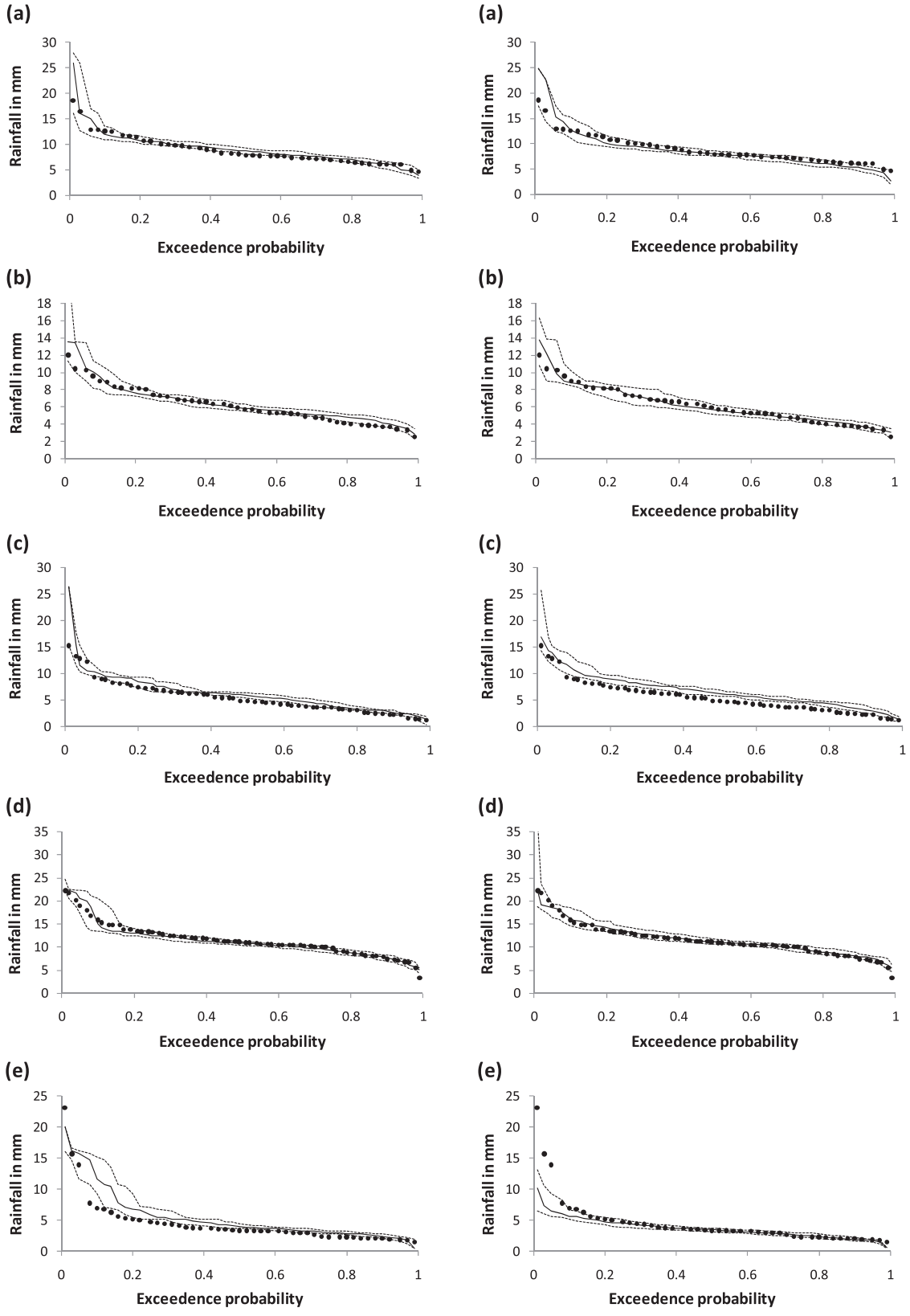

Figure 9. Six-minute annual maximum rainfall against exceedance probability for (a) Sydney, (b) Perth, (c) Alice Springs, (d) Cairns, and (e) Hobart. Black dots represents observed data, black solid line represents the median of 100 simulations, and black dotted lines represent the 5th- and 95th-percentile simulated values.

than resulting in a deterioration in performance, it is likely that the regionalized version actually provides a better representation of the sampling intervals for these very large events.

[49] In addition to the results presented in Figure 9 for the 6-min duration annual maxima, we also tabulated the results for other durations up to 12 h, presented in Table 4. Once again, the observed and simulated sequences are generally similar, with the median-sampled value within 10% of the observed value, and no obvious systematic under- or overestimation biases. The exception here is for Hobart, in which the annual maxima are typically undersimulated by 10%–20%. It should be noted, however, that the observed rainfall often falls outside of the 5th- and 95th-percentile simulation bounds, highlighting that the simulation bounds may underestimate the true level of variance. Finally, although the results are only presented in Table 4 for the regionalized method of fragments, the results from the at-site implementation are comparable, again highlighting that the regionalized method of fragments does not result in any notable deterioration in model performance.

[50] We next consider the antecedent rainfall prior to the design storm burst event, plotted in Figure 10. The justification for focusing on the antecedent rainfall exceedance probability plot was because of the often important relationship between the "flood-producing" rainfall event and the catchment wetness prior to the event [*Kuczera et al.*, 2006]. We only focus on the 6-h antecedent rainfall depth, as antecedent conditions for longer durations (particularly, multiday antecedent rainfall depth) will be correctly captured as we are using observed daily rainfall data at the location of interest.

[51] As can be seen, the simulated data appear to follow the observed data reasonably well, although there are several points outside the 90% sampling interval. Importantly, no systematic biases could be identified, with performance varying depending on the location. This is also shown in the lower half of Table 4 with the antecedent rainfall of different durations prior to the 1-h storm burst. The observed antecedent rainfall is generally within the 90% sampling interval, with the exception of Cairns in which antecedent rainfall is underestimated for 6-h depth prior to the 1-h storm burst, and overestimation for longer durations. Once again, the main outlier is for Hobart Airport, however, as discussed in the context of the annual maxima this is likely due to a recording error for the pluviograph record.

[52] Finally, we present results addressing the connectivity in rainfall events between successive wet days. This is a potential issue with the conventional method of fragments logic described in the literature [*Lall and Sharma*, 1996; *Nowak et al.*, 2010; *Sharma et al.*, 1997; *Snavidze*, 1977; *Tarboton et al.*, 1998], as the subdaily fragments are, in effect, randomly reordered such that by definition all of the within-day rainfall characteristics will be preserved, but the between-day characteristics will be lost other than ensuring that the daily total rainfalls are maintained. This was one of the primary justifications for using the state-based method of fragments, in which the fragments are selected conditional on both current day wetness and the previous and next-day wetness state.

[53] The results are presented in Table 5 for all five test locations. For each location, the first four rows represent the probability that the last hour of day t (represented as $X_{t,24}$) is wet or dry given that the next day is wet or dry.

Table 4. Comparison of Observed and Simulated Results for Median Annual Maxima for Different Storm Burst Durations and Antecedent Rainfall Prior to 1 h Storm Burst[a]

	Sydney		Perth		Alice Springs		Cairns		Hobart	
	Observed	Simulated (5% and 95% Bounds)	Observed	Simulated (5% and 95% Bounds)	Observed	Simulated (5% and 95% Bounds)	Observed	Simulated (5% and 95% Bounds)	Observed	Simulated (5% and 95% Bounds)
					Annual Maxima					
6 min	8.9	8.8 (8.14–9.32)	6.2	6.2 (5.77–6.81)	5.5	6.8 (6.32–7.2)	11.6	11.8 (11.15–12.65)	4.5	3.8 (3.4–4.12)
30 min	25.7	23.7 (21.95–25.92)	14.7	14.0 (13.08–15.26)	16.7	18.2 (17.09–19.45)	34.9	35.3 (33.96–37.05)	11.3	8.9 (8.22–9.55)
1 h	35.4	32.6 (30.04–35.45)	18.8	18.4 (16.95–19.72)	22.1	24.2 (22.5–25.75)	51.7	51.9 (49.76–54.79)	14.6	12.0 (11.26–12.85)
3 h	55.4	49.4 (46.46–52.47)	29.0	27.9 (26.18–29.89)	32.6	33.6 (31.42–35.16)	83.5	85.1 (81.33–89)	22.9	19.5 (18.54–20.56)
6 h	72.3	64.0 (61.08–67.09)	36.3	35.4 (34.09–37.53)	39.6	39.8 (37.65–41.42)	113.0	110.8 (106.12–114.22)	30.3	26.5 (25.69–27.75)
12 h	91.8	84.8 (81.92–87.2)	45.4	44.5 (43.46–45.63)	48.2	46.5 (45.42–47.65)	147.4	140.7 (137.24–144.39)	39.6	35.3 (34.58–36.26)
					Antecedent Moisture Prior to 1-h Burst (mm)					
6 h	15.4	13.2 (9.86–17.13)	6.8	8.5 (6.26–10.06)	6.1	5.3 (4.14–6.91)	25.4	21.5 (17.97–26.25)	6.3	5.2 (4.21–6.52)
12 h	22.7	18.8 (14.61–23.34)	9.7	10.9 (8.17–12.93)	8.0	7.8 (5.97–9.73)	32.3	31.0 (25.15–35.9)	9.1	6.8 (5.52–8.59)
24 h	31.4	28.1 (22.51–35.5)	12.8	13.6 (11.12–16.64)	10.7	11.5 (8.7–13.5)	42.0	49.1 (40.99–56.76)	10.2	9.0 (7.1–11.55)
48 h	43.0	37.2 (29.05–46.59)	15.5	17.2 (14.01–20.82)	15.5	16.8 (12.99–19.96)	58.6	74.3 (63.77–86.02)	11.4	11.1 (8.33–14.19)

[a]The simulated median annual maxima represent the median of all 100 simulations.

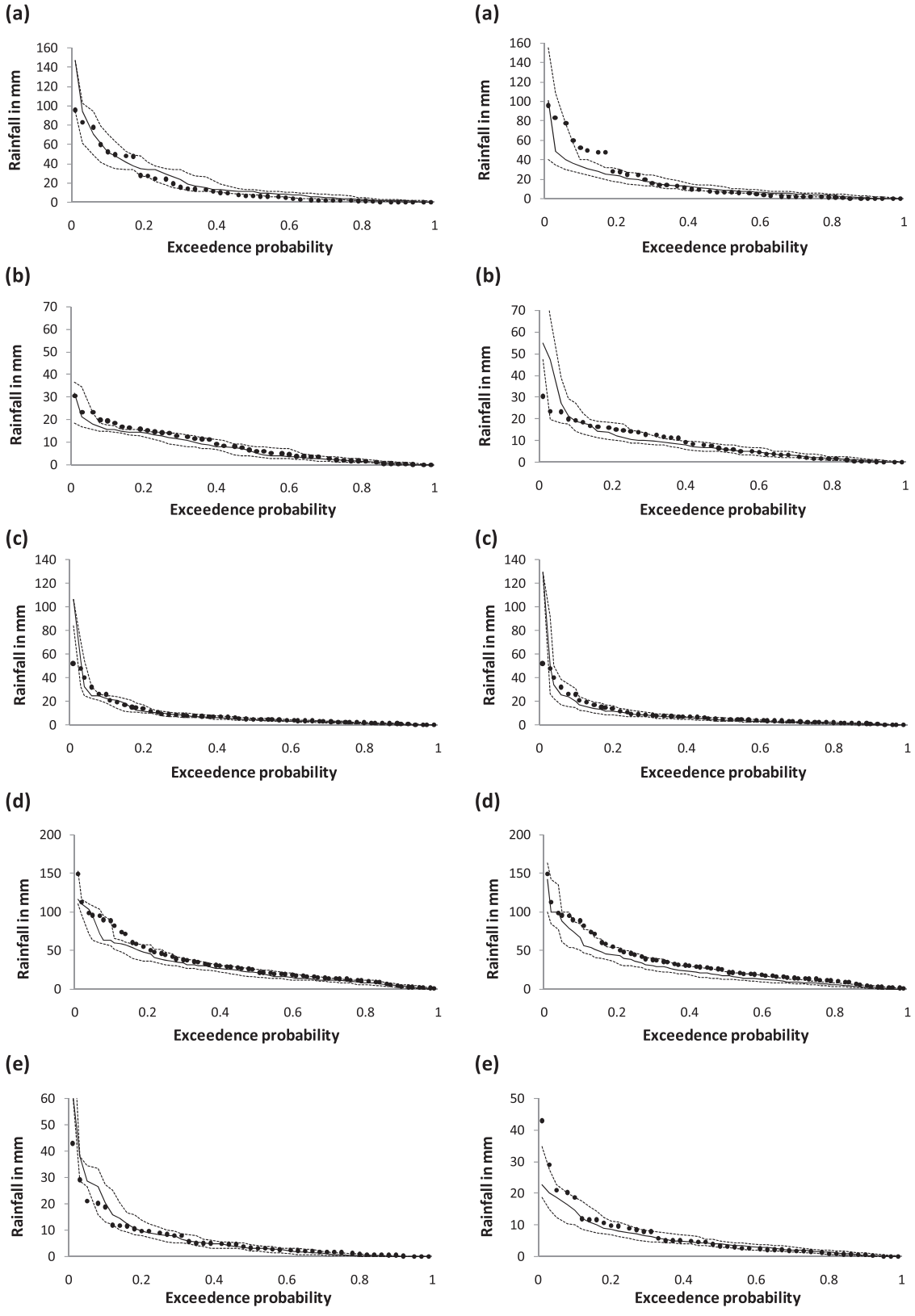

Figure 10. Six hour antecedent rainfall prior to the 6-min annual maximum storm burst plotted against exceedance probability for (a) Sydney, (b) Perth, (c) Alice Springs, (d) Cairns, and (e) Hobart. Black dots represents observed data, black solid line represents the median of 100 simulations, and black dotted lines represent the 5th- and 95th-percentile simulated values.

Table 5. The Connectivity of Rainfall Spells Between Successive Wet Days[a]

Location Data	Observed	Conventional MoF[b]	State-Based MoF
	Sydney Airport		
$\Pr(X_{t,24} > 0, R_{t+1} > 0 \mid R_t > 0)$	19.9%	13.1%	18.3%
$\Pr(X_{t,24} > 0, R_{t+1} = 0 \mid R_t > 0)$	5.2%	11.2%	6.4%
$\Pr(X_{t,24} = 0, R_{t+1} > 0 \mid R_t > 0)$	28.0%	34.9%	29.7%
$\Pr(X_{t,24} = 0, R_{t+1} = 0 \mid R_t > 0)$	46.9%	40.8%	45.6%
$\Pr(X_{t,24}>0, X_{t+1,1} > 0 \mid R_t > 0, R_{t+1} > 0)$	31.7%	6.7%	14.7%
	Perth Airport		
$\Pr(X_{t,24} > 0, R_{t+1} > 0 \mid R_t > 0)$	21.6%	15.9%	21.3%
$\Pr(X_{t,24} > 0, R_{t+1} = 0 \mid R_t > 0)$	5.2%	11.7%	7.4%
$\Pr(X_{t,24} = 0, R_{t+1} > 0 \mid R_t > 0)$	30.9%	36.5%	31.1%
$\Pr(X_{t,24} = 0, R_{t+1} = 0 \mid R_t > 0)$	42.3%	35.9%	40.2%
$\Pr(X_{t,24}>0, X_{t+1,1} > 0 \mid R_t > 0, R_{t+1} > 0)$	26.7%	6.8%	14.3%
	15590		
$\Pr(X_{t,24} > 0, R_{t+1} > 0 \mid R_t > 0)$	16.3%	6.5%	11.3%
$\Pr(X_{t,24} > 0, R_{t+1} = 0 \mid R_t > 0)$	6.7%	7.9%	4.0%
$\Pr(X_{t,24} = 0, R_{t+1} > 0 \mid R_t > 0)$	24.8%	34.6%	29.7%
$\Pr(X_{t,24} = 0, R_{t+1} = 0 \mid R_t > 0)$	52.2%	51.0%	55.0%
$\Pr(X_{t,24}>0, X_{t+1,1} > 0 \mid R_t > 0, R_{t+1} > 0)$	28.6%	2.4%	8.3%
	31011		
$\Pr(X_{t,24} > 0, R_{t+1} > 0 \mid R_t > 0)$	21.2%	15.4%	19.8%
$\Pr(X_{t,24} > 0, R_{t+1} = 0 \mid R_t > 0)$	3.6%	6.4%	4.3%
$\Pr(X_{t,24} = 0, R_{t+1} > 0 \mid R_t > 0)$	44.0%	49.9%	45.4%
$\Pr(X_{t,24} = 0, R_{t+1} = 0 \mid R_t > 0)$	31.2%	28.4%	30.5%
$\Pr(X_{t,24}>0, X_{t+1,1} > 0 \mid R_t > 0, R_{t+1} > 0)$	20.9%	5.3%	8.9%
	94008		
$\Pr(X_{t,24} > 0, R_{t+1} > 0 \mid R_t > 0)$	14.0%	9.6%	14.5%
$\Pr(X_{t,24} > 0, R_{t+1} = 0 \mid R_t > 0)$	4.4%	10.4%	5.6%
$\Pr(X_{t,24} = 0, R_{t+1} > 0 \mid R_t > 0)$	30.1%	34.5%	29.6%
$\Pr(X_{t,24} = 0, R_{t+1} = 0 \mid R_t > 0)$	51.4%	45.5%	50.2%
$\Pr(X_{t,24}>0, X_{t+1,1} > 0 \mid R_t > 0, R_{t+1} > 0)$	23.6%	4.5%	10.9%

[a]The first four rows provide the probability that the last hour of day t ($X_{t,24}$) is wet/dry given that the next day $t + 1$ is wet/dry, with the probabilities summing to 100%. The fifth row is the probability that the last hour of day t, and the first hour of day $t + 1$ wet.
[b]MoF, Method of Fragments.

This has been calculated for the observed record as well as for the conventional and state-based implementations of the method of fragments logic. As can be seen, the state-based logic yields a significant improvement compared with the conventional method of fragments. In particular, the probability that the last hour of the day is wet is underestimated by the conventional method of fragments when the next day is wet, and overestimated when the next day is dry, for all five locations.

[54] The fifth row then summarizes the probability that the last hour of day t, and the first hour of day $t + 1$, are both wet for successive wet days. As can be seen, this is dramatically underestimated for both the conventional and state-based method of fragments, highlighting that the temporal patterns on the boundary between wet days are likely to be less continuous for the simulated data compared with the observations. Nevertheless, the state-based method of fragments provides a significant improvement compared with the conventional algorithm, highlighting the advantages of moving to the state-based logic.

5. Discussion and Conclusions

[55] In this paper, a framework was described where continuous (6-min increment) rainfall can be generated at any location of interest provided that daily data is either available or can be synthetically generated. The basis of this approach is randomly to draw subdaily fragments from nearby pluviograph stations conditional on the daily rainfall amount and the previous- and next-day wetness state at the target station. The identification of nearby stations is based on a distance metric which considers latitude and longitude as well as elevation and distance to coast, with the relative importance of each variable determined by looking at the similarity in the daily-to-subdaily scaling at 232 long pluviograph stations across Australia.

[56] The approach sought to address several important limitations associated with the Australian pluviograph record. First, compared to daily rainfall data, there is approximately one order of magnitude less pluviograph stations, and the records at each station are usually much shorter than their daily read counterparts. Thus, by combining longer, more abundant, and more reliable daily data at the target location with the information contained in a number of pluviograph records in the neighborhood of the target location, it is possible to make the best use of the both types of data. Second, by drawing records from multiple nearby pluviograph records rather than relying on a single record, it is also possible to consider information from records only several years long, which would usually be discarded as being too short for meaningful analysis. Finally, pluviograph data flagged as missing or unreliable can simply be discarded from the analysis, even for cases where there is a systematic bias in the missing data (e.g., pluviograph recording tends to

fail during major storm events). This is because, provided the daily rainfall data are reliable, and there are sufficient data at other pluviograph stations to capture a diversity of rainfall events across a range of magnitudes, such possible systematic pluviograph recording biases are unlikely to be translated into the final synthetically generated sequences.

[57] The evaluation of the method on a range of statistics which are relevant for flood estimation, notably the annual maximum statistics and the antecedent rainfall prior to the flood-producing storm burst, suggests that the method compares reasonably well with at-site data for the five test locations considered. In particular, no significant deterioration in the results could be observed when moving from the at-site method of fragments to the regionalized version, suggesting that the regionalized version properly represents the at-site variability. Furthermore, it is likely that the sampling intervals for the regionalized version are likely to more reasonably reflect the true variability of the data, with widening sampling intervals for lower exceedance probability (and thus higher magnitude) events; although, as discussed in the context of the results of Table 4, this variability may still be underestimated. This also highlights that the regionalized method is able to provide a much greater diversity of extreme rainfall sequences (and associated temporal patterns) than what has been observed at any one point location, with this in turn likely to yield more robust flood-frequency results when the continuous rainfall sequences are run through a continuous rainfall-runoff model.

[58] We also looked at the connectivity in the temporal patterns between successive wet days, which represents one of the most obvious limitations of the method of fragments logic. In general, the state-based logic proposed here results in a notable improvement in connectivity, although it is clear that the method is unable to reproduce observed connectivity exactly. Nevertheless, the implications for applications such as flood estimation are unclear. For example, if the method is able to reproduce within-day temporal patterns, preserves annual maximum rainfall and associated antecedent conditions, and maintains the daily total rainfall depths, then the effect of some discontinuities on flood estimates are unlikely to be large. The use of these generated sequences as an input for continuous rainfall-runoff modeling would be one way to test this issue, and is an area which we plan to investigate further.

[59] We note that like most continuous simulation algorithms, the objective of our method is to preserve various statistics of historical rainfall variability. We have addressed nonstationarity in the daily-to-subdaily scaling as a result of seasonal fluctuations by selecting fragments from within the same season. We do not expect that non-stationarity issues due to inter-annual variability of rainfall are likely to result in major distortions to the fidelity of the generated continuous sequences, since much of this variability results in changes to wet day occurrences and daily rainfall amounts rather than sub-daily temporal patterns [*Pui et al.*, 2011b]. Thus, this should be accounted for by the daily rainfall simulation algorithm rather than the daily to subdaily disaggregation approach. Finally, there is an increased interest in nonstationarity of rainfall (and other hydroclimatic sequences) as a result of anthropogenic climate change [e.g., *Milly et al.*, 2008]. In particular, the associated increases in temperature may be expected to yield more intense rainfall bursts for a given daily rainfall amount [e.g., see *Hardwick-Jones et al.*, 2010; *Lenderink and van Meijgaard*, 2008; *Lenderink et al.*, 2011; *Westra and Sisson*, 2011], however, explicitly addressing this issue is reserved for future research.

[60] Although daily data is much more abundant than pluviograph data across Australia, in many regions the length or reliability of daily rainfall may not be sufficient for the stochastic generation of rainfall sequences. This is the subject of the next paper, in which the approach presented here is generalized to any location in Australia, regardless of the availability of daily or pluviograph data.

[61] **Acknowledgments.** This study was supported by an Australian Research Council Discovery grant as well as a research grant from the Institution of Engineers, Australia to help develop continuous rainfall sequences for design flood estimation. The daily and continuous rainfall records used were obtained from the Australian Bureau of Meteorology. Finally, we wish to thank Geoff Pegram and two anonymous reviewers, whose comments and suggestions have greatly improved the quality of the manuscript.

References

Blazkova, S., and K. Beven (2002), Flood frequency estimation by continuous simulation for a catchment treated as ungauged (with uncertainty), *Water Resour. Res.*, *38*(8), 1139, doi:10.1029/2001WR000500.

Boughton, W., and O. Droop (2003), Continuous simulation for design flood estimation—a review, *Environ. Model. Software*, *18*(4), 309–318.

Cameron, D., K. Beven, J. Tawn, and P. Naden (2000), Flood frequency estimation by continuous simulation (with likelihood based uncertainty estimation), *Hydrol. Earth Syst. Sci.*, *4*(1), 23–34.

Cowpertwait, P. S. P., and P. E. O'Connell (1997), A regionalised Neyman-Scott model of rainfall with convective and stratiform cells, *Hydrol. Earth Syst. Sci.*, *1*, 71–80.

Cowpertwait, P. S. P., P. E. O'Connell, A. V. Metcalfe, and J. A. Mawdsley (1996), Stochastic point process modelling of rainfall. II. Regionalisation and disaggregation, *J. Hydrol.*, *175*, 47–65.

Cowpertwait, P. S. P., V. Isham, and C. Onof (2007), Point process models of rainfall: Developments for fine-scale structure, *Proc. R. Soc. A and B*, *463*(2086), 2569–2588.

Fasano, G., and A. Franceschini (1987), A multidimensional version of the Kolmogorov-Smirnov test, *Monthly Notices of the Royal Astronomical Society*, *225*, 155–170.

Frost, A. J., R. Srikanthan, and P. S. P. Cowpertwait (2004), Stochastic generation of rainfall data at subdaily timescales: A comparison of DRIP and NSRP, *Rep. 04/9*, pp. 1813–1819, CRC, Salisbury South, Australia.

Gupta, V. K., and E. C. Waymire (1993), A statistical analysis of mesoscale rainfall as a random cascade, *J. Appl. Meteorol.*, *32*, 251–267.

Gyasi-Agyei, Y. (1999), Identification of regional parameters of a stochasic model for rainfall disaggregation, *J. Hydrol.*, *223*, 148–163.

Gyasi-Agyei, Y., and S. M. Parvez Bin Mahbub (2007), A stochastic model for daily rainfall disaggregation into fine time scale for a large region, *J. Hydrol.*, *347*, 358–370.

Gyasi-Agyei, Y., and G. R. Willgoose (1997), A hybrid model for point rainfall modelling, *Water Resour. Res.*, *33*(7), 1699–1706.

Gyasi-Agyei, Y., and G. R. Willgoose (1999), Generalisation of a hybrid model for point rainfall, *J. Hydrol.*, *219*(3–4), 218–224.

Hardwick-Jones, R., S. Westra, and A. Sharma (2010), Observed relationships between extreme sub-daily precipitation, surface temperature and relative humidity, *Geophys. Res. Lett.*, *37*, L22805, doi:10.1029/2010GL045081.

Hastie, T., R. Tibshirani, and J. Friedman (2009), *The Elements of Statistical Learning: Data Mining, Inference and Prediction*, 763 pp., Springer, Berlin, Germany.

Koutsoyiannis, D., and C. Onof (2001), Rainfall disaggregation using adjusting procedures on a Poisson cluster model, *J. Hydrol.*, *246*(1–4), 109–122.

Kuczera, G., M. Lambert, T. M. Heneker, S. Jennings, A. J. Frost, and P. J. Coombes (2006), Joint probability and design storms at the crossroads, *Aust. J. Water Resour.*, *10*(1), 63–80.

Lall, U., and A. Sharma (1996), A nearest neighbour bootstrap for resampling hydrological timeseries, *Water Resour. Res.*, *32*, 679–693.

Lamb, R., and A. L. Kay (2004), Confidence intervals for a spatially generalized, continuous simulation flood frequency model for Great Britain, *Water Resour. Res.*, *40*(7), W07501, doi:10.1029/2003WR002428.

Lenderink, G., and E. van Meijgaard (2008), Increase in hourly precipitation extremes beyond expectations from temperature changes, *Nat. Geosci.*, *1*, 511–514.

Lenderink, G., H. Y. Mok, T. C. Lee, and G. J. Van Oldenborgh (2011), Scaling and trends of hourly precipitation extremes in two different climate zones—Hong Kong and the Netherlands, *Hydrol. Earth Syst. Sci.*, *8*, 4701–4719.

Lovejoy, S., and D. Schertzer (1990), Multifractals, universality classes, and satellite and radar measurements of cloud and rain fields, *J. Geophys. Res.*, *95*, 2021–2031.

Marshak, A., A. Davis, R. Cahalan, and W. Wiscombe (1994), Bounded cascade models as nonstationary multifractals, *Phys. Rev. E*, *49*(1), 55–69.

Mehrotra, R., and A. Sharma (2006), Conditional resampling of hydrologic time series using multiple predictor variables: A *K*-nearest neighbour approach, *Adv. Water Resour.*, *29*, 987–999.

Menabde, M., D. Harris, A. W. Seed, G. Austin, and D. Stow (1997), Multiscaling properties of rainfall and bounded random cascades, *Water Resour. Res.*, *33*(12), 2823–2830.

Milly, P. C. D., J. Betancourt, M. Falkenmark, R. M. Hirsch, W. Zbigniew, Z. W. Kundzewicz, D. P. Lettenmaier, and R. J. Stouffer (2008), Stationarity is dead: Whither water management?, *Science*, *319*, 573–574.

Nowak, K., J. Prarie, B. Rajagopalan, and U. Lall (2010), A nonparametric stochastic approach for multisite disaggregation of annual to daily streamflow, *Water Resour. Res.*, *46*, W08529, doi:10.1029/2009WR008530.

Press, W. H., S. A. Teukolsky, W. T. Vetterling, and B. P. Flannery (1992), *Numerical Recipes in Fortran—The Art of Scientific Computing*, 2nd ed., 963 pp., Cambridge Univ. Press, Cambridge, Mass.

Pui, A., A. Lall, and A. Sharma (2011a), How does the Interdecadal Pacific Oscillation affect design floods in Australia?, *Water Resour. Res.*, *47*, W05554, doi:10.1029/2010WR009420.

Pui, A., S. Westra, A. Santoso, and A. Sharma (2011b), Impact of the El Niño Southern Oscillation, Indian Ocean Dipole, and Southern Annular Mode on daily to sub-daily rainfall characteristics in East Australia, *Monthly Weather Review*, in press.

Rodriguez-Iturbe, I., D. Cox, and V. Isham (1987), Some models for rainfall based on stochastic point processes, *Proc. R. Soc. A and B*, *410*, 269–288.

Rodriguez-Iturbe, I., D. Cox, and V. Isham (1988), A point process model for rainfall: Further developments, *Proc. R. Soc. A and B*, *417*, 283–298.

Schertzer, D., and S. Lovejoy (1987), Physical modelling and analysis of rain and clouds by anisotropic scaling multiplicative processes, *J. Geophys. Res.*, *92*, 9693–9714.

Sharma, A., and R. Srikanthan (2006), Continuous rainfall simulation: A nonparametric alternative, in 30th Hydrology and Water Resour. Symp., Launceston, Tasmania.

Sharma, A., D. G. Tarboton, and U. Lall (1997), Streamflow simulation: a nonparametric approach, *Water Resour. Res.*, *33*(2), 291–308.

Snavidze, G. G. (1977), *Mathematical Modeling of Hydrologic Series*, 314 pp., Water Resour. Publ., Littleton, Colo.

Tarboton, D. G., A. Sharma, and A. Lall (1998), Disaggregation procedures for stochastic hydrology based on nonparametric density estimation, *Water Resour. Res.*, *34*(1), 107–119.

Verhoest, N., P. Troch, and F. D. Troch (1997), On the applicability of Bartlett-Lewis rectangular pulse models in the modelling of design storms at a point, *J. Hydrol.*, *202*, 108–120.

Westra, S., and S. A. Sisson (2011), Detection of non-stationarity in precipitation extremes using a max-stable process model, *J. Hydrol.*, *406*, 119–128.

R. Mehrotra and A. Sharma, School of Civil and Environmental Engineering, University of New South Wales, Sydney, NSW 2052, Australia. (a.sharma@unsw.edu.au)

R. Srikanthan, Water Division, Australian Bureau of Meterology, G.P.O. Box 1289, Melbourne, Victoria 3001, Australia.

S. Westra, School of Civil, Environmental, and Mining Engineering, University of Adelaide, SA 5005, Australia.